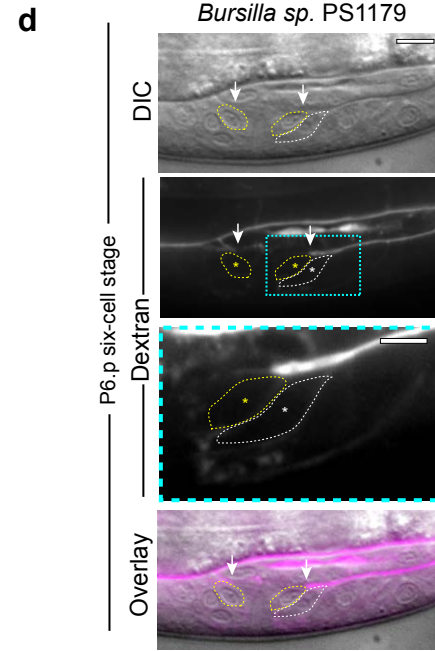
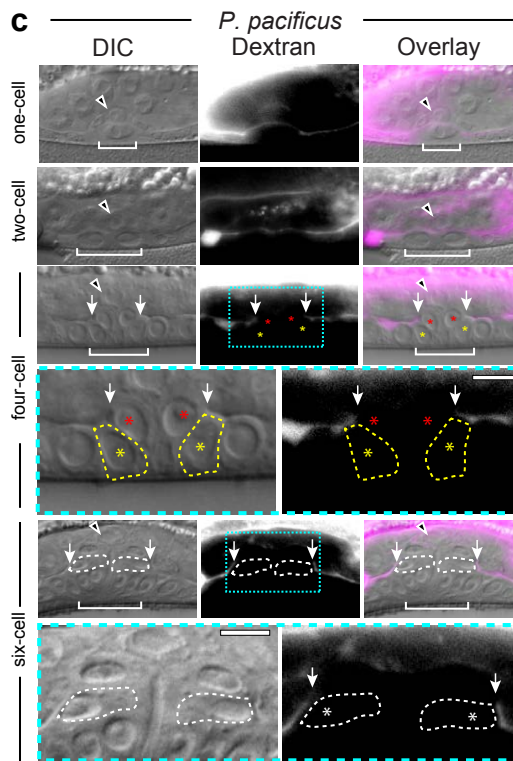
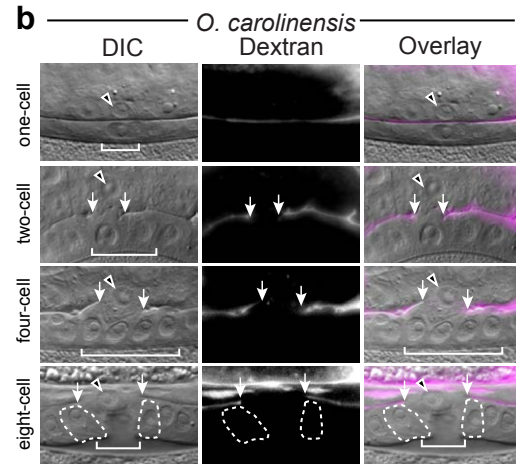
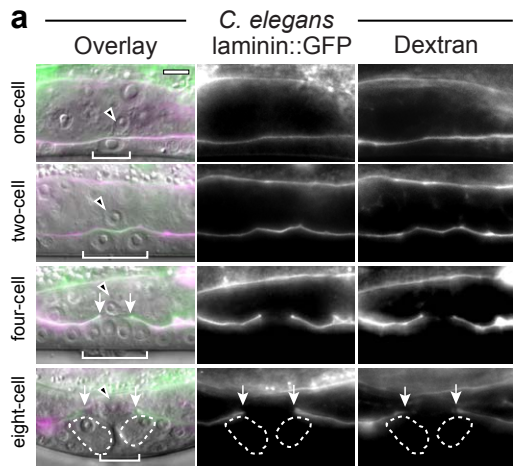


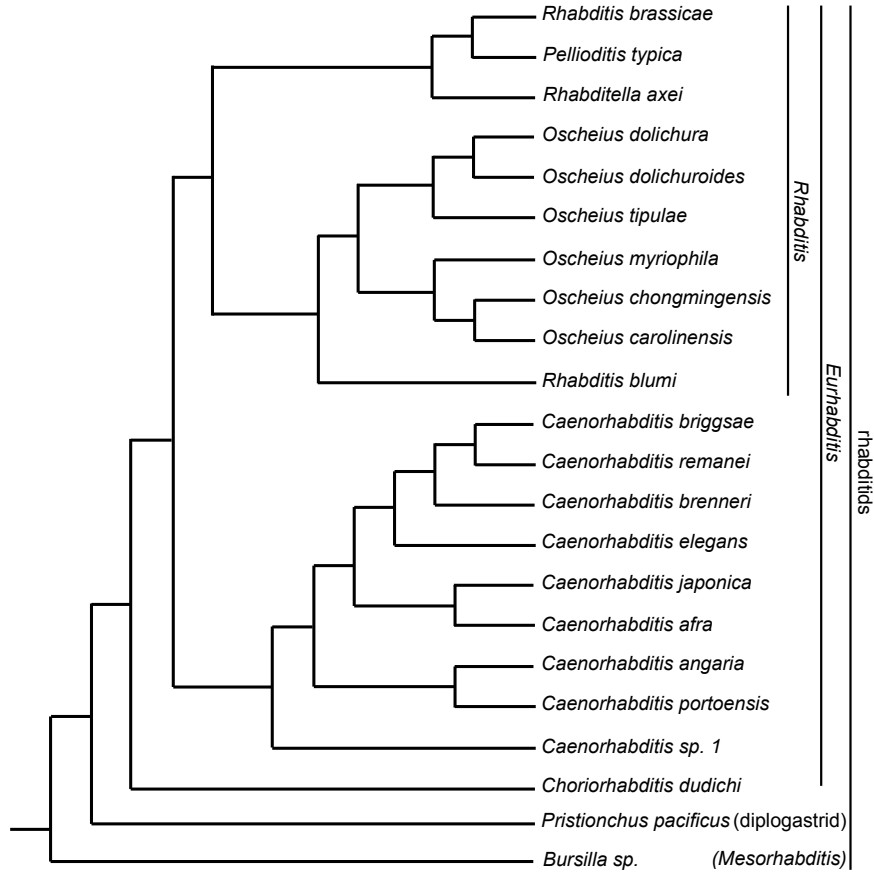
Supplementary Figure 1. Rhabditid nematode AC invasion occurs prior to initiation of

vulval invagination. DIC microscopy of twenty species of rhabditid nematodes. DIC micrographs depict the position of the AC (black arrowhead), width of the BM breach (yellow arrowheads, partial invasion; white arrows, full invasion) and division stage of P6.p (white bracket) at the P6.p one- (left), two- (middle), and four-cell stage (right; $n \geq 50$ animals examined for each stage and species; see Supplementary Table 1 for scoring data). Colors differentiate between those species that invade “early” (in relation to P6.p divisions) at the late P6.p one- (red text) or the early two-cell stage (orange) and those that invade “late” at the late P6.p two- (green) and the early P6.p four-cell stage (blue). Scale bar, 5 μm .



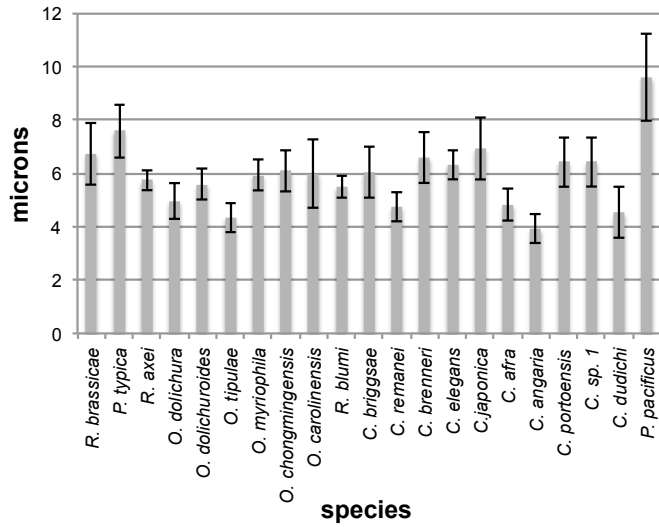
Supplementary Figure 2. Rhodamine dextran injections label the BM. (a-c) DIC micrographs (left), corresponding fluorescence showing BM laminin::GFP (a, middle) or rhodamine dextran (a, right; b,c, middle), and DIC images with rhodamine dextran fluorescence overlaid (b,c, right). DIC micrographs depict the position of the AC (black arrowhead), width of the BM breach (white arrows), division stage of P6.p (white bracket) and position of the D cell at the P6.p eight-cell stage (dashed lines). (a) A *C. elegans* strain with the BM labeled with laminin::GFP (middle) injected with rhodamine dextran at the P6.p one-, two-, four-, and eight-cell stages (right) showed that rhodamine dextran specifically labels the BM and colocalizes with laminin::GFP (a, left). (b) *Oscheius carolinensis* rhodamine dextran injections revealed a BM breach at the P6.p two-cell stage (middle column, fluorescence overlay right column) and the BM boundary positioned over the D cell. (c) *Pristionchus pacificus* rhodamine dextran injections revealed a BM breach at the P6.p four-cell stage and the BM gap boundary resided over the D cells at the P6.p eight-cell stage (dashed lines, white asterisks, dashed blue line inset shows magnified view). At the P6.p four-cell stage the BM gap boundary was over the E cells (yellow asterisks), extending beyond the non-dividing F cells (red asterisks). (d) The BM stabilized over the post-mitotic vulE precursor cells in *Bursilla sp.* (PS1179). DIC image (top), corresponding confocal section of the BM labeled with rhodamine dextran (middle panels, dashed blue line inset shows magnified view) and DIC image overlay (bottom) of P6.p six-cell stage animal. Dashed white lines and white asterisks indicate the position of the D cell. The BM gap boundary position (white arrows) resided over the post-mitotic E cell (yellow asterisks and dashed yellow line, n = 5 for each stage and species). Scale bars, 5 μ m.

a

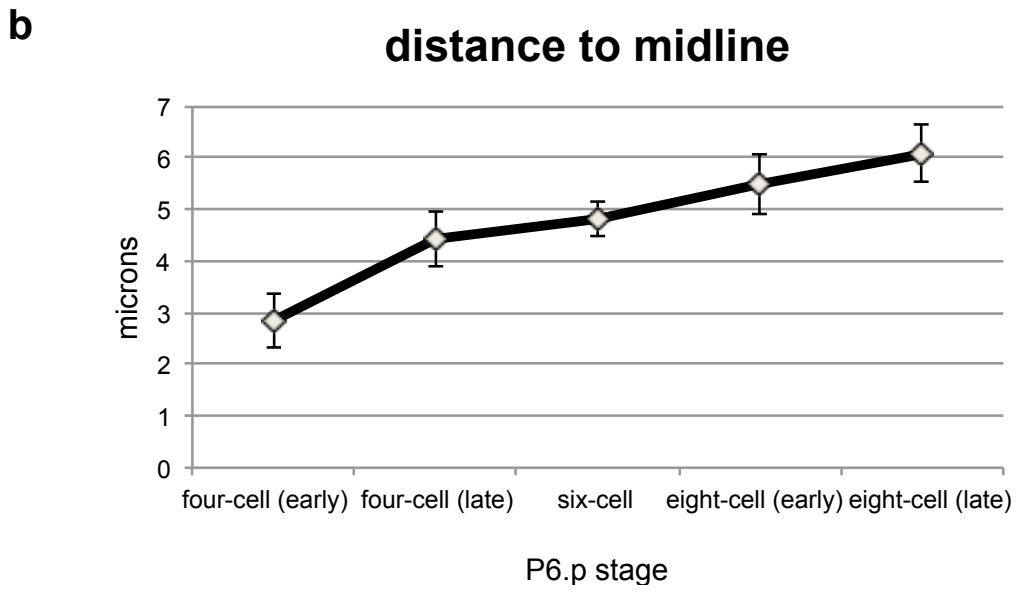
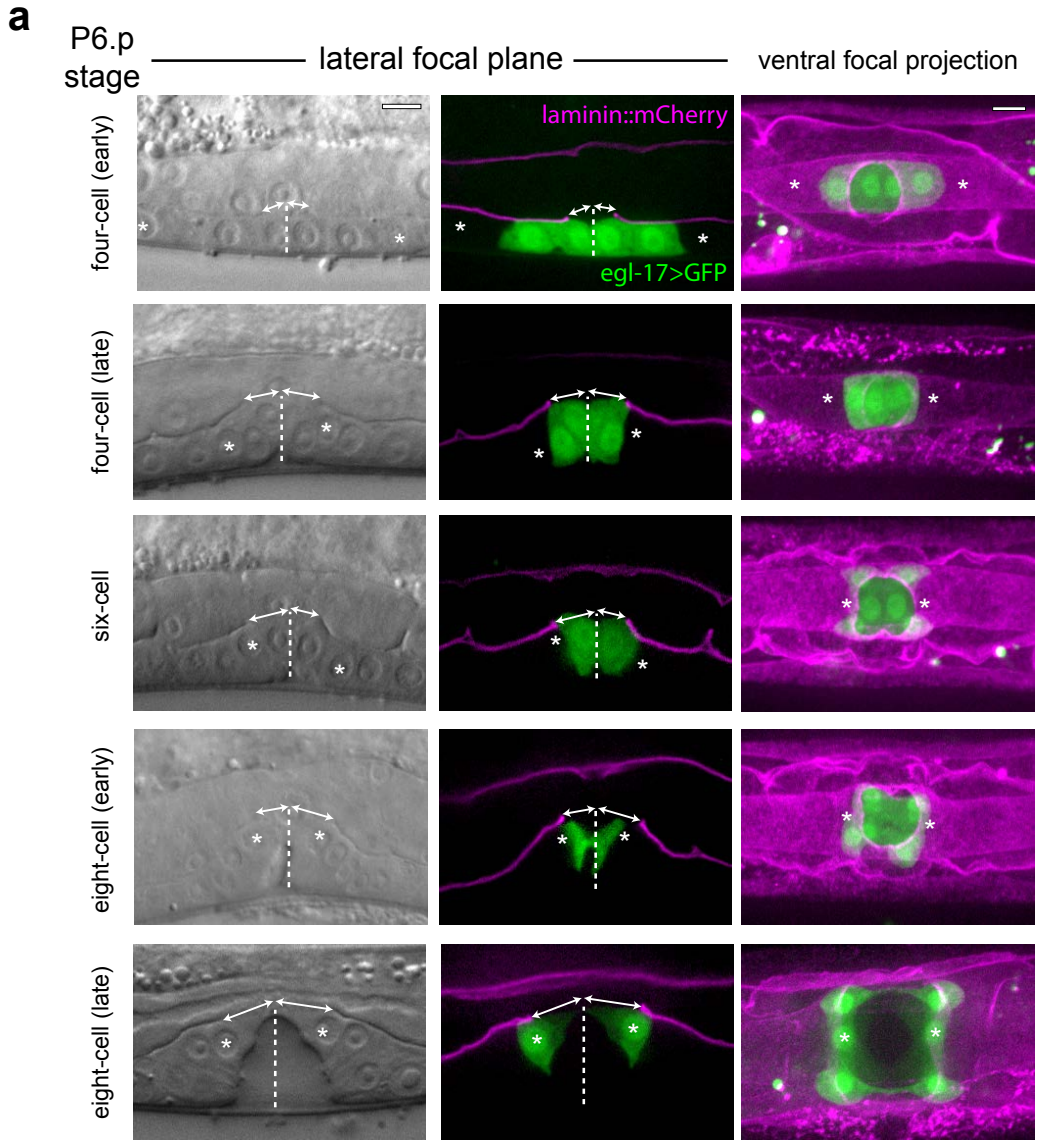


distance to midline

b

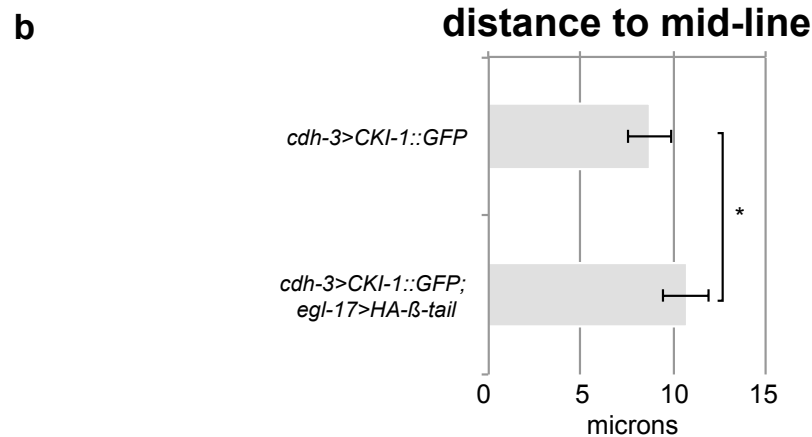
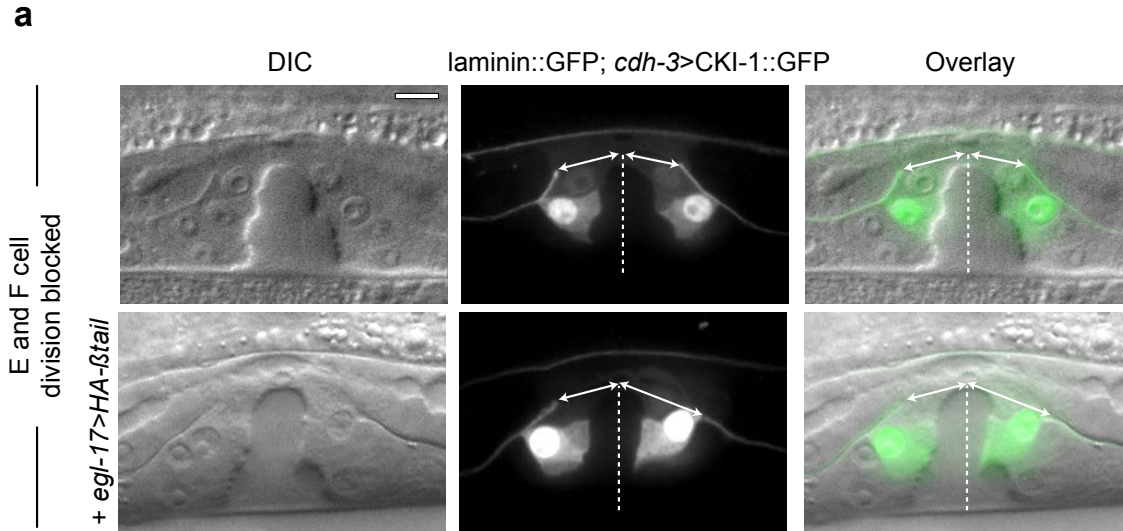


Supplementary Figure 3. Phylogenetic relationships of species examined and quantification of BM gap boundary distance. (a) Rhabditid nematode phylogeny of species examined in this study (based on ²⁰⁻²³). (b) Quantification of the distance in microns between the vulval midline and BM gap edge in each rhabditid species at the late P6.p eight-cell stage (n ≥ 6 examined for each species, error bars represent s.d.).

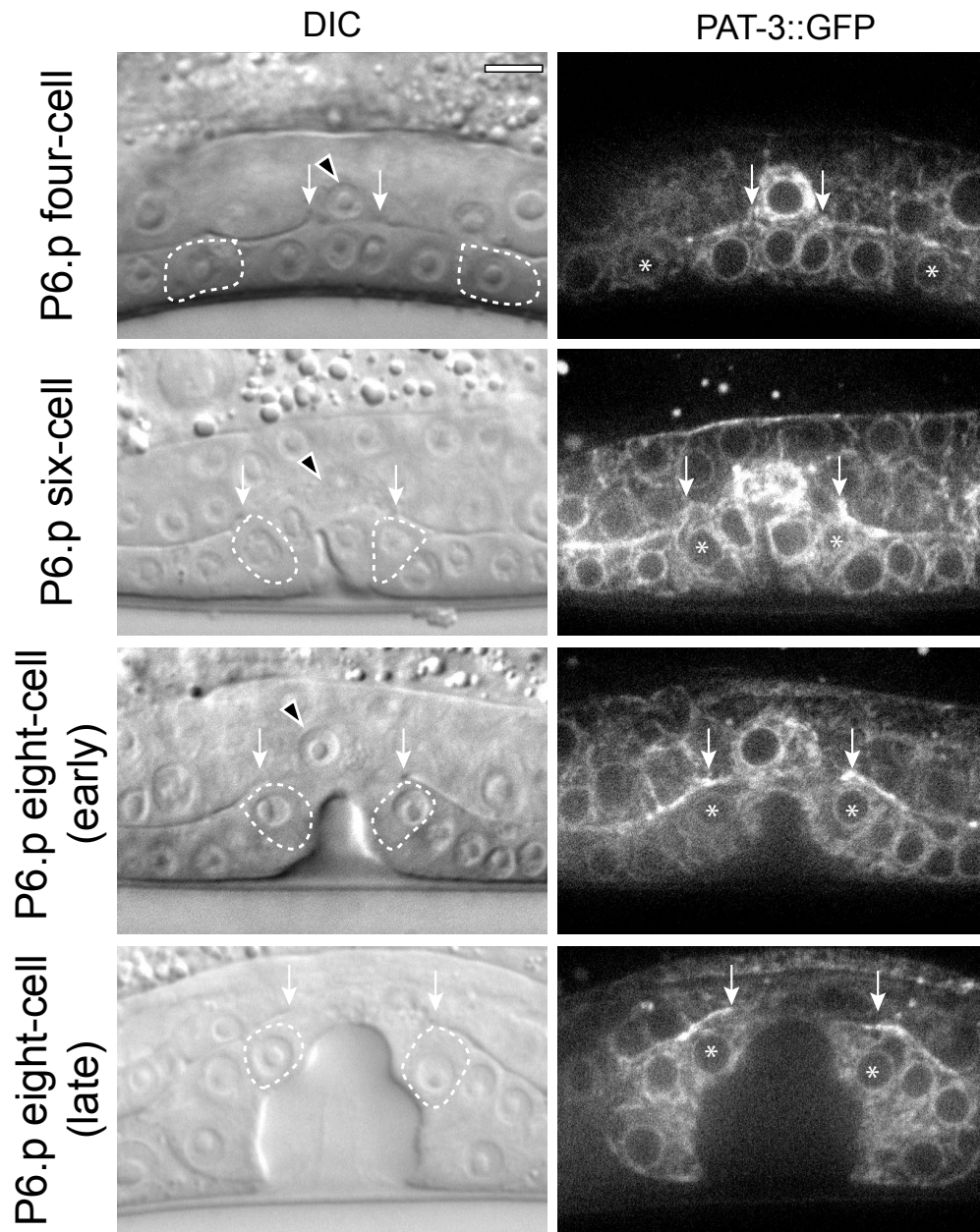


Supplementary Figure 4. Quantification of BM gap boundary distance over

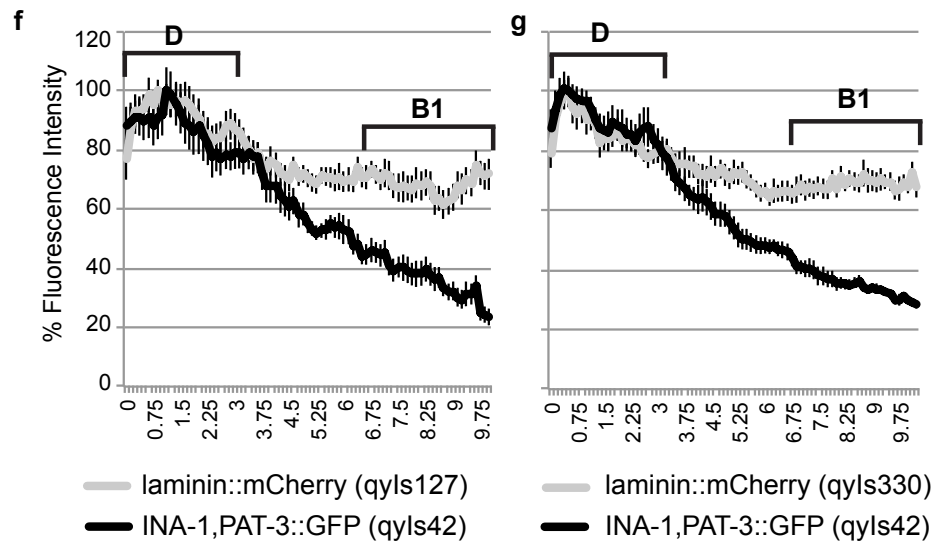
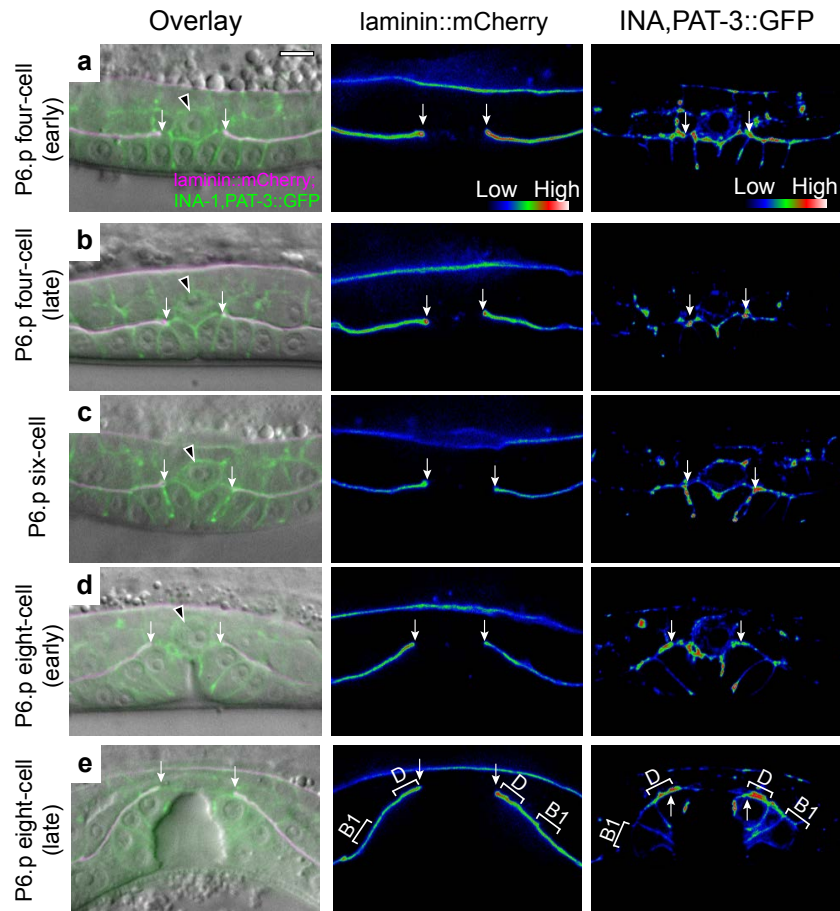
developmental time. (a) DIC micrographs (left), and corresponding single lateral confocal optical section showing BM (laminin::mCherry) and position of VPCs (*egl-17*>GFP expressed in the E and F cells initially (P6.p four-cell through early eight-cell stage) and then in the C and D cells at the late P6.p eight-cell stage) and a corresponding 3-D reconstruction of a confocal z-stack showing a ventral view of BM gap expansion (right). Dashed line indicates position of the vulval midline and white double arrows indicate measured distance from the midline to the edge of the BM gap and white asterisk denotes position of the D cell. Confocal images for ventral views were acquired using an EM-CCD digital camera (iXon Ultra, Andor) and a spinning disk confocal microscope (CSU-X1; Yokogawa) mounted on a compound microscope (Nikon Ti; Nikon) with a Plan-APOCHROMAT 100x/1.45 oil differential interference contrast objective and controlled by Metamorph software (Molecular Devices). (b) Quantification of the distance in microns between the vulval midline and BM gap edge across development time (stages correspond to images shown in (a), n = 18, 44, 16, 12, and 14 examined for each stage, respectively, error bars represent s.d.). Scale bar, 5 μ m.



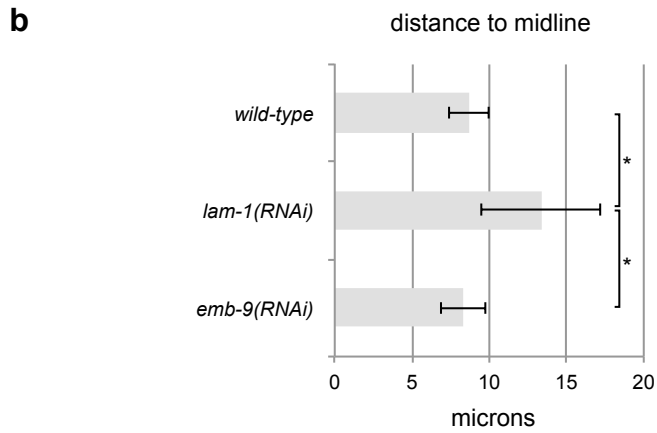
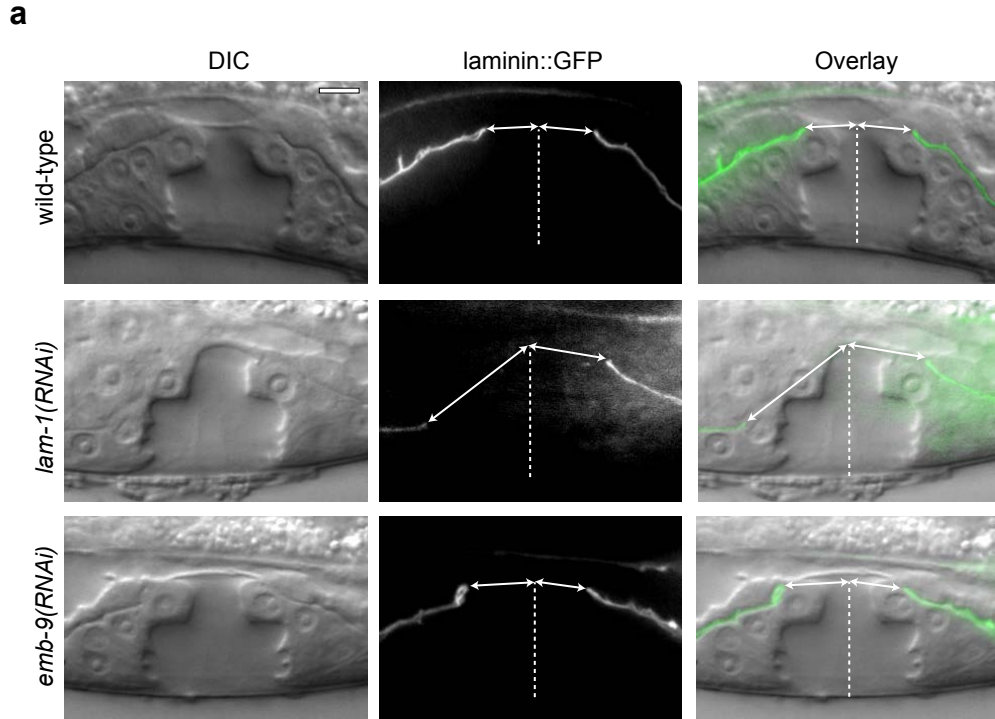
Supplementary Figure 5. Quantification of BM gap boundary distance in relation to blocked E and F cell divisions. (a) DIC micrographs (left) and corresponding confocal fluorescence (middle) and overlay (right) depicting BM gap distance at the P6.p late eight-cell stage following prevention of E and F cell divisions (expressing *cdh-3>CKI-1::GFP*; top). Perturbation of integrin function (*egl-17>HA-βtail*, bottom) resulted in BM gap expansion. Dashed line indicates position of the vulval midline and white double arrows indicate measured distance from the midline to the edge of the BM gap. (b) Quantification of the distance in microns between the vulval midline and BM gap edge between blocked E and F cell divisions (n = 16 (top) and n = 19 (bottom), **P* < 0.0001, Student's *t* test, error bars represent s.d.) Scale bar, 5 μm.



Supplementary Figure 6. A *pat-3::GFP* translational reporter is expressed uniformly in the VPCs. DIC images (left) and corresponding confocal sections (right) of expression of a *pat-3* translational reporter (*pat-3::GFP*) showed uniform expression in all the VPCs at the P6.p four-, six-, and eight-cell stages. DIC micrographs depict the position of the AC (black arrowhead), width of the BM breach (white arrows), and position of the D cells (dashed lines, left; asterisk, right). n = 10 examined for each stage of vulval development). Scale bar, 5 μ m.

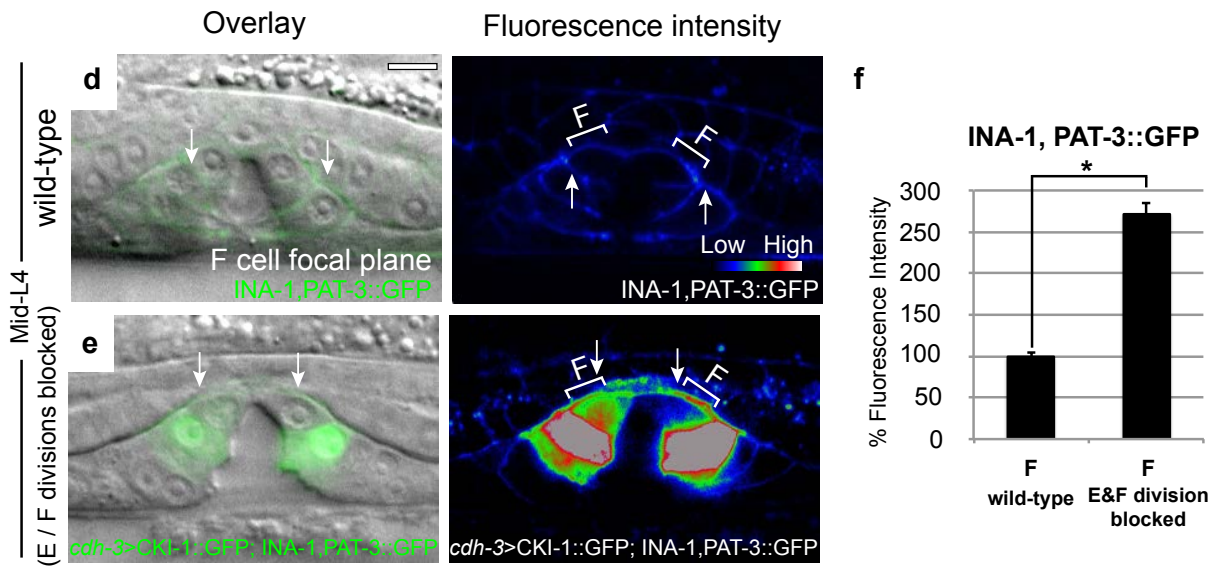
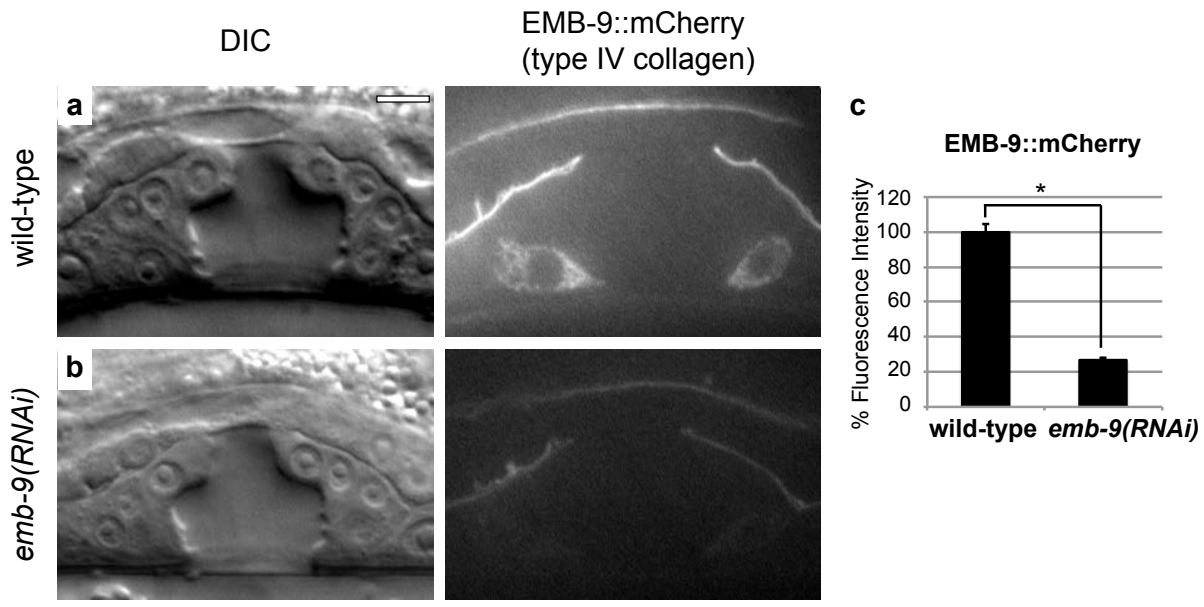


Supplementary Figure 7. Laminin and integrin transgene quantification during uterine-vulval attachment. (a-e) DIC micrographs (left) overlaid with BM fluorescence (laminin::mCherry, magenta), integrin (INA-1,PAT-3::GFP, green) and corresponding confocal sections showing spectral representations of fluorescence intensity of laminin::mCherry (middle) and INA-1,PAT-3::GFP (right). AC position is indicated by the black arrowhead. Spectral representation of laminin::mCherry fluorescence revealed enriched laminin signal at the BM gap edge (white arrows) from the early P6.p four-cell stage through the late P6.p eight-cell stage. Enriched integrin (INA-1,PAT-3::GFP) fluorescence at the D cell-BM interface was observed at the late P6.p eight-cell stage (mid-L4) (e). (f,g) Quantification (shown as mean \pm s.e.m.) of the average fluorescence intensity of INA-1,PAT-3::GFP (qyls42, black) and laminin::mCherry (qyls127(f), qyls330(g), grey) across a 10.25 μ m long, 5 pixel wide line scan from the BM gap edge to the B1 cell-BM interface (see Methods; n = 14 cases observed). Black bars represent the location of the D and B1 cell-BM interface. Scale bar, 5 μ m.

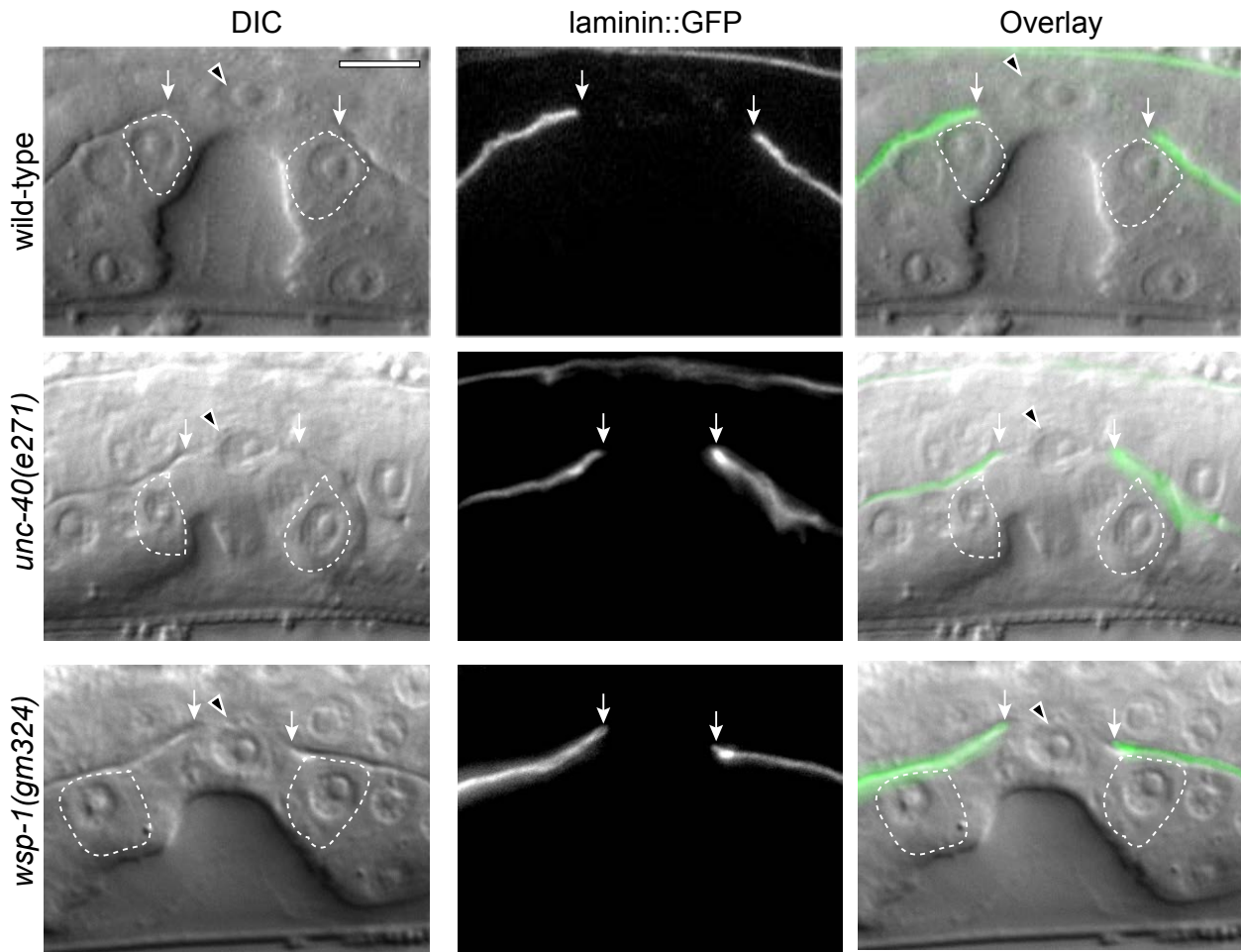


Supplementary Figure 8. Quantification of BM gap boundary distance following RNAi

depletion of BM components. (a) DIC micrographs (left) and corresponding confocal fluorescence images (middle) and overlay (right) depicting representative images used to quantify BM gap distance (double arrows) to vulval midline (dashed line). (b) Quantification of the distance in microns between the vulval midline and BM gap edge (n = 28 (top), n = 11 (middle), n = 24 (bottom), * $P < 0.003$, Student's t test, error bars represent s.d.). Scale bar, 5 μm .



Supplementary Figure 9. Type IV collagen and integrin quantification. DIC micrographs (left) and corresponding confocal sections of the BM viewed with EMB-9::mCherry (α -1 chain of type IV collagen; right). (a,b) Comparison of fluorescence intensity of EMB-9::mCherry (shown as mean \pm s.e.m.) in wild-type (a) and an *emb-9(RNAi)* depleted animal (b) at the late L4 stage. (c) Depletion of *emb-9* by RNAi resulted in an 83% reduction in EMB-9::mCherry fluorescence intensity along the BM (n = 12 animals for each; * $P < 1.0e-14$, Student's t-test) but did not alter BM gap position (see Figure 6I). (d-f) Comparison of the fluorescence intensity of the integrin INA-1, PAT-3::GFP at the basal surface of (d) divided F cells and (e) blocked E and F cell divisions (using *cdh-3*>CKI-1::GFP, which was downregulated in the F cells as compared to the D cells at the P6.p eight-cell stage (mid-L4 stage), allowing for quantification of fluorescence intensity at the F cell – BM interface). (f) Quantification (shown as mean \pm s.e.m.) of 3.375 μ m line scans (white brackets) revealed a significant 2.7 fold increase in INA-1, PAT-3::GFP localization within non-divided F cells where the BM was halted (n = 14 cases observed for each; * $P < 1.0e-09$; Student's *t* test). Scale bars, 5 μ m.



Supplementary Figure 10. AC invasion mutants show BM gap expansion defect. DIC micrographs (left) and corresponding confocal sections of the BM viewed with laminin::GFP (middle) and overlay (right) depicting narrow BM opening in mutants that show a delay in BM breach (white arrows, wild-type(top); *unc-40(e271)*, middle and *wsp-1(gm324)*, bottom). Black arrowhead indicates the AC and dashed lines indicate the position of the D cells. Scale bar, 5 μm .

Supplementary Tables

Supplementary Table 1. Scoring table of timing of the BM breach in *C. elegans* and twenty other species of rhabditid nematodes

Strain Designation	Species	P6.p two-cell stage			P6.p four-cell stage			Count
		No Invasion	Partial Invasion	Invasion	No Invasion	Partial Invasion	Invasion	Total
DF5006	<i>R. axei</i> *	0 (0%)	0 (0%)	51 (100%)	0 (0%)	0 (0%)	56 (100%)	107
CEW1	<i>O. tipulae</i> *	0 (0%)	7 (12.07%)	51 (87.93%)	0 (0%)	0 (0%)	50 (100%)	108
YEW1	<i>O. carolinensis</i>	3 (5.88%)	8 (15.69%)	40 (78.43%)	0 (0%)	0 (0%)	50 (100%)	101
AF13	<i>O. chongmingensis</i>	0 (0%)	8 (14.29%)	48 (85.71%)	0 (0%)	0 (0%)	52 (100%)	108
DF5033	<i>O. dolichura</i>	20 (40%)	15 (30%)	15 (30%)	0 (0%)	0 (0%)	62 (100%)	112
DF5025	<i>P. typica</i>	10 (19.61%)	4 (7.84%)	37 (72.55%)	0 (0%)	0 (0%)	68 (100%)	119
DF5010	<i>R. blumi</i>	0 (0%)	14 (27.45%)	37 (72.55%)	0 (0%)	0 (0%)	59 (100%)	110
SB193	<i>R. brassicae</i>	0 (0%)	8 (15.38%)	44 (84.62%)	0 (0%)	0 (0%)	55 (100%)	107
DF5020	<i>O. myriophila</i>	50 (92.59%)	4 (7.41%)	0 (0%)	0 (0%)	0 (0%)	62 (100%)	116
PS1010	<i>C. angaria</i>	31 (60.78%)	20 (39.22%)	0 (0%)	0 (0%)	7 (11.67%)	53 (88.33%)	111
AF16	<i>C. briggsae</i>	49 (98%)	1 (2%)	0 (0%)	0 (0%)	0 (0%)	56 (100%)	106
SB122	<i>C. dudichi</i>	45 (90%)	5 (10%)	0 (0%)	0 (0%)	0 (0%)	56 (100%)	106
N2	<i>C. elegans</i>	50 (87.72%)	7 (12.28%)	0 (0%)	0 (0%)	0 (0%)	50 (100%)	107
DF5081	<i>C. japonica</i>	47 (94%)	3 (6%)	0 (0%)	0 (0%)	5 (9.80%)	46 (90.20%)	101
JU1667	<i>C. species 1</i>	41 (82%)	9 (18%)	0 (0%)	0 (0%)	0 (0%)	52 (100%)	102
EG4788	<i>C. portoensis</i>	47 (92.16%)	4 (7.84%)	0 (0%)	0 (0%)	2 (3.45%)	56 (96.55%)	109
JU1199	<i>C. afra</i>	60 (86.96%)	9 (13.04%)	0 (0%)	0 (0%)	0 (0%)	50 (100%)	119
PB2801	<i>C. brenneri</i>	50 (100%)	0 (0%)	0 (0%)	4 (7.02%)	5 (8.77%)	48 (84.21%)	107
SB146	<i>C. remanei</i>	56 (100%)	0 (0%)	0 (0%)	0 (0%)	0 (0%)	55 (100%)	111
DF5018	<i>O. dolichuroides</i>	50 (100%)	0 (0%)	0 (0%)	0 (0%)	2 (3.03%)	64 (96.97%)	116
PS312	<i>P. pacificus</i>	50 (100%)	0 (0%)	0 (0%)	0 (0%)	0 (0%)	51 (100%)	101

* denotes species with P6.p one-cell stage partial invasion scored:

Species	P6.p one-cell stage			Count
	No Invasion	Partial Invasion	Invasion	Total
<i>R. axei</i>	50 (88.68%)	10 (7.55%)	2 (3.77%)	62
<i>O. tipulae</i>	53 (81.54%)	12 (18.46%)	0%	65

Supplementary Table 2. BM gap position during vulval development

(a) wild-type, (b) *cdh-3>CKI-1::GFP* animals where E and F cell divisions were blocked, (c) *cdh-3>CKI-1::GFP; HA-β-tail* animals (E and F cell divisions blocked and perturbed integrin signaling), (d) RNAi targeting BM components

a. BM gap position in wild-type animals (Related to Figure 4)

P6.p cell stage	BM gap position				Total cases observed
	E/F cell	D cell	B2 cell	A cell	
four-cell (early)	26	0	0	0	26
four-cell (late)	45	11	0	0	56
six-cell	22	28	0	0	50
eight-cell (early)	0	32	0	0	32
eight-cell (late)	0	40	0	0	40

b. BM gap position in *cdh-3>CKI-1::GFP* animals (Related to Figures 5a-e)

P6.p cell stage	BM gap position				Total cases observed
	E/F cell	D cell	B2 cell	A cell	
four-cell (early)	40	0	0	0	40
four-cell (late)	22	0	0	0	22
six-cell	54	2	0	0	56
eight-cell (early)	46	6	0	0	52
eight-cell (late)	32	9	0	0	41

c. BM gap position in *cdh-3>CKI-1::GFP; HA-β-tail* animals (Related to Figures 5f-j)

P6.p cell stage	BM gap position				Total cases observed
	E/F cell	D cell	B2 cell	A cell	
four-cell (early)	28	0	0	0	28
four-cell (late)	13	1	0	0	14
six-cell	40	1	1	0	42
eight-cell (early)	37	7	2	0	46
eight-cell (late)	11	17	4	0	32

d. BM gap position following RNAi targeting BM components at the P6.p eight-cell stage (late L4 stage) (Related to Figures 6g-i)

RNAi target	BM gap position			Total cases observed	
	E/F cell	D cell	B2 cell		A cell
wild-type / empty-vector	0	20	0	0	20
<i>lam-1</i> (laminin)	0	18	8	2	28
<i>emb-9</i> (type IV collagen)	0	20	0	0	20

Supplementary Table 3. Extrachromosomal arrays and integrated strains generated

Ex designation	Is designation	PCR fusion created	Injected concentration	Coinjection marker
qyEx240	qyls229	<i>cdh-3</i> > <i>H2B::GFP</i> ^a	0.1 ng ml ⁻¹	unc-119+
qyEx269	qyls266	<i>cdh-3</i> > <i>CKI-1::GFP</i> ^b	0.1 ng ml ⁻¹	unc-119+
qyEx241	qyls232	<i>CDT-1::GFP</i> ^b	0.2 ng ml ⁻¹	unc-119+
qyEx366	qyls351	<i>unc-62</i> > <i>GFP::CAAX</i> ^a	0.1 ng ml ⁻¹	unc-119+

^a 3' UTR from the *nmy-2* gene was included at the 3' end of the construct

^b The endogenous 3' UTR was used

Supplementary Table 4. Primer sequences and templates used for all PCR fusions generated

Primer sequence	Primer type	Amplicon	Template
5'-ggTTTgTAgAATgTgTTgTTCC-3'	<i>forward</i>	<i>cdh-3</i> promoter (5kb)	JP38
5'-CTCATATCgAAggTTCTgTgTCC-3'	<i>forward nested</i>	<i>cdh-3</i> promoter (5kb)	JP38
5'-CgTATTgTCATCTATTCAGCATTgATCTgg-3'	<i>reverse</i>	<i>cdh-3</i> promoter (5kb)	JP38
5'-gAATAgATgACAATACgATgTCTTCTgCTCgTC-3'	<i>cdh-3 extension, forward</i>	H2B::GFP	pLZ6
5'-TCATAgAgATATgCACCCATAC-3'	<i>reverse</i>	H2B::GFP	pLZ6
5'-TCAATATgCggTgTACTTCTgg-3'	<i>reverse nested</i>	H2B::GFP	pLZ6
5'-gAATAgATgACAATACgATgCCACCAAAGCCATCTg-3'	<i>cdh-3 extension, forward</i>	CKI-1::GFP	fosmid WRM0626bF02
5'-gTCCgTTCCAAggTCTTCTCg-3'	<i>reverse</i>	CKI-1::GFP	fosmid WRM0626bF02
5'-TCACgCAATCTTCACgCAATgTC-3'	<i>reverse nested</i>	CKI-1::GFP	fosmid WRM0626bF02
5'-TTgACACCgTTCTCTgAgCTgg-3'	<i>forward</i>	CDT-1::GFP	N2 genomic DNA
5'-TgAgACCgCgAgggAAAgC-3'	<i>forward nested</i>	CDT-1::GFP	N2 genomic DNA
5'-AAgTTCTTCTCCTTTACTCATATgAAATTTgAgAgATC-3'	<i>gfp extension, reverse</i>	CDT-1::GFP	N2 genomic DNA
5'-ATgAgTAAAggAgAAgAACTTTTCAC-3'	<i>forward</i>	GFP	pPD95_81
5'-CTCgCgCgTTTCgTgATgACgTgA-3'	<i>reverse</i>	GFP	pPD95_81
5'-CTACTAgTCggCCgTACgggCCCTT 3'	<i>reverse nested</i>	GFP	pPD95_81
5'-CTTgCAgAACATgATgAgTAAAggAgAAgAAC-3'	<i>unc-62 extension, forward</i>	GFP::CAAX	pSA129
5'-CTTACCgCTgTTgAgATCCAgTTC-3'	<i>reverse</i>	GFP::CAAX	pSA129
5'-gggAATAAgggCgACACggAAATg-3'	<i>reverse nested</i>	GFP::CAAX	pSA129
5'-ATgTAgCTgCCAgCCATggATA-3'	<i>forward</i>	<i>unc-62</i> promoter (3kb)	fosmid WRM061dC01
5'-CAAAAgtCATATATCATgACAgATTAggAgg-3'	<i>forward nested</i>	<i>unc-62</i> promoter (3kb)	fosmid WRM061dC01
5'-CATgTTCCgCAAgAgAAATATTA-3'	<i>reverse</i>	<i>unc-62</i> promoter (3kb)	fosmid WRM061dC01